Magnetic clustering of weakly interacting Ni-ions in Ni-exchanged zeolites

Graphical Abstract

MAGNETIC CLUSTERING OF WEAKLY INTERACTING Ni-IONS IN Ni-EXCHANGED ZEOLITES

Gabriele Barrera, Paolo Allia, Paola Tiberto, Olimpia Tammaro, Michele Pansini, Antonello Marocco, Maela Manzoli, Giorgia Confalonieri, Rossella Arletti, Serena Esposito

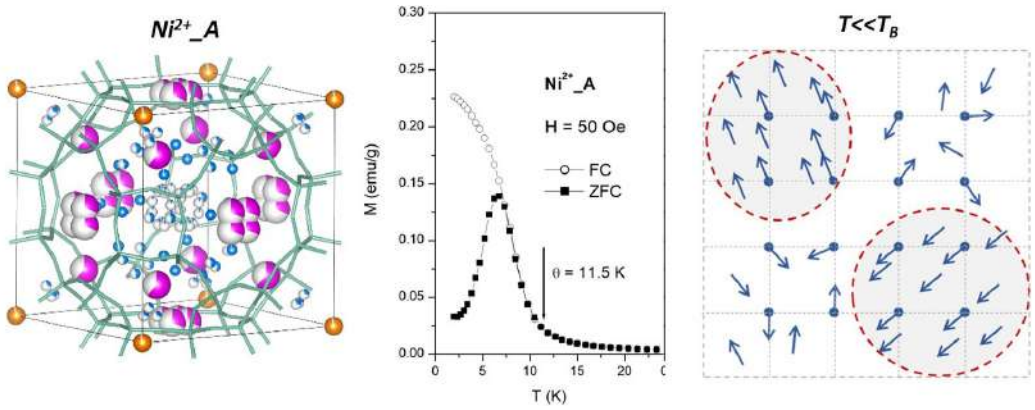

Highlights

MAGNETIC CLUSTERING OF WEAKLY INTERACTING Ni-IONS IN Ni-EXCHANGED ZEOLITES

Gabriele Barrera, Paolo Allia, Paola Tiberto, Olimpia Tammaro, Michele Pansini, Antonello Marocco, Maela Manzoli, Giorgia Confalonieri, Rossella Arletti, Serena Esposito

- Comprehensive picture of temperature-dependent magnetic regimes in Ni-loaded zeolites
- Weakly interacting Ni cations evenly distributed in the zeolite structure
- Independent magnetic clusters formed below 11 K by effect of magnetic interaction
- Magnetic clusters exhibit superparamagnetic-blocked state transition around 6 K
- Size and properties of magnetic clusters determined by magnetic (SQUID) measurements

MAGNETIC CLUSTERING OF WEAKLY INTERACTING Ni-IONS IN Ni-EXCHANGED ZEOLITES

Gabriele Barrera[a,*], Paolo Allia[a], Paola Tiberto[a], Olimpia Tammaro[b], Michele Pansini[c], Antonello Marocco[c], Maela Manzoli[d], Giorgia Confalonieri[e], Rossella Arletti[f], Serena Esposito[b,**]

[a] *INRIM, Advanced Materials Metrology and Life Sciences, Strada delle Cacce 91, Torino, 10135, Italy*

[b] *Politecnico di Torino, DISAT, and INSTM Unit, Corso Duca degli Abruzzi 24, Torino, 10129, Italy*

[c] *Universit*

ΩΩimmediateà degli Studi di Cassino e del Lazio Meridionale, Civil and Mechanical Engineering, and INSTM Unit, Via G. Di Biasio 43, Cassino, 03043, Italy

[d] Universitit

ΩΩimmediateà degli Studi di Torino, Drug Science and Technology, NIS and INSTM Reference Centres, Via P. Giuria 9, Torino, 10125, Italy

[e] ID22 beamline, European Synchrotron Radiation Facility (ESRF), 71 Av. des Martyrs, Grenoble, 38000, France

[f] Universit

ΩΩimmediateà degli Studi di Modena e Reggio Emilia, Chemical and Geological Sciences, Via Campi 103, Modena, 41125, Italy

Abstract

Divalent Nickel cations were incorporated in two commercial zeolites (Na-A zeolite and Na-X zeolite) by a process of ionic exchange marginally affecting structure, morphology and porosity of the host materials, as verified by XRD, HRTEM and physisorption measurements. Comparable amounts of magnetic ions were introduced (4.80 wt.% in Na-A zeolite and 6.20 wt.% in Na-X zeolite), as checked by AAS and TGA. Magnetic measurements were done between 2 and 300 K using a SQUID magnetometer up to 70 kOe. The

*Corresponding Author: g.barrera@inrim.it

**Corresponding Author: serena_esposito@polito.it

initial susceptibility follows the Curie-Weiss law with Curie temperatures θ of 10.3 and 11.5 K. The effective magnetic moments on Ni^{2+} ions suggest almost complete quenching of the angular momentum. No long-range magnetic order is found below θ; however, FC/ZFC magnetization curves indicate the formation of superparamagnetic clusters of magnetic ions with blocking temperature of about 6.5 K in both zeolites. Cluster size, average number of clustered ions, effective anisotropy of clusters are evaluated. A comprehensive picture of all magnetic effects taking place over the whole temperature range is drawn by combining magnetic, structural and morphological data.

Keywords: Ni-exchanged zeolites, Magnetic porous materials, Short-range magnetic ordering, Magnetic clustering, Superparamagnetism
PACS: 82.75.vx, 75.20.ck, 36.40.cg

1. Introduction

Zeolites and zeolite-based materials find application in a variety of industrial and research areas [1, 2] such as catalysis [3], separation processes [4], environmental remediation [5, 6], hydrogen storage [7]. By incorporating active species in the zeolitic scaffold, new composite materials are produced which combine the physico-chemical properties of the zeolites with the ones of the dispersed guest species, thereby enhancing their functionalities [1].

In particular, insertion of transition metal species in porous materials such as zeolites by either impregnation or ion exchange results in novel environment-friendly [8] or catalyst materials [9, 10] such as the ones used in organic-chemistry processes (e.g., methane-to-methanol conversion [11], ethylene oligomerization [12, 13], l-butene dimerization [14] acetylene hydrogenation [15], phytase immobilization [16]). In addition, zeolites incorporating transition metal ions are key precursors of nanocomposites containing ferromagnetic nanoparticles of transition metals such as Fe^0, Ni^0, Co^0obtained by suitable thermal treatments. These nanomaterials have been exploited as sorption catalysts in CO_2 hydrogenation processes [17] or as magnetoceramics where the starting zeolite structure has collapsed [18] with applications in biological entity separation [19, 20], environmental sciences [21, 22], lunar soil simulants [23, 24]. The functional properties of all materials (both precursors and by-products) critically depend on the distribution of transition metal ions in the zeolitic scaffold; as a consequence, a detailed study of the physical properties of magnetic ions is the starting point for an in-depth

assessment of the performance of the final products.

Nickel is one of the most investigated transition metals which can be incorporated in zeolites [15, 25, 26, 27, 28]. In particular, the effects of temperature and number of ionic exchanges on the incorporation of Ni cations and on both structure and thermal stability of zeolites A,X, and Y have been elucidated in a detailed study [25]. Together with the structural properties, the magnetic properties of these porous materials with different fractions of incorporated cations have been investigated in some detail [27, 28, 29, 30, 31, 32]. The most recent works have been done on metal-ceramic nanocomposites produced by submitting Ni-exchanged zeolites to suitable thermal treatments in an affordable process which exhibits potential for practical application owing to low cost, efficiency, simplicity and versatility [33, 34, 35]. In these ceramic materials, a non-negligible fraction of magnetic ions is still present even after the collapse of the zeolitic structure and the simultaneous formation of magnetic nanoparticles, almost independently of the type of host zeolite. The residual ionic fraction is larger in materials incorporating a higher starting fraction of Ni cations [27, 28]. The magnetic properties of the nanocomposites are particularly hard to interpret owing to the compresence of signals stemming from magnetic nanoparticles and from the residual phase of interacting cations, whose contribution strongly increases with decreasing temperature. Instead, Ni-exchanged zeolites do not contain magnetic nanoparticles prior to thermal treatment; therefore, a study of zeolites loaded with Ni can give a safer detailed picture of the actual distribution of cations in the zeolitic scaffold.

In this work, the magnetic properties of two Ni-exchanged, porous zeolites (A and X zeolite) incorporating comparable fractions of Ni^{2+} ions (of the order of 5 wt%) are studied over an extended temperature interval. The interpretation of magnetic data is supported by Atomic Absorption Spectrophotometry, X-ray Powder Diffraction and Transmission Electron Microscopy complemented by information about porosity and water physisorption. Measurements of the initial magnetic susceptibility show that the materials are paramagnetic around room temperature and follow a Curie-Weiss law; a weak ferromagnetic interaction among dispersed cations is responsible for the onset of magnetic clusters below the Curie temperature ($\approx$ 11 K in both materials). Magnetic clusters exhibit a superparamagnetic behaviour with blocking temperature around 6.5 K. The results allow us to get a complete picture of the magnetic effects in these loaded zeolites and to draw conclusions about the actual placement of magnetic ions in the zeolitic scaffold.

2. EXPERIMENTAL

Carlo Erba reagent grade 4A zeolite (framework type LTA [36], formula $Na_{12}Al_{12}Si_{12}O_{48} \cdot 27\ H_2O$, hereafter referred to as "Na-A zeolite") and 13X zeolite (framework type FAU [36], $Na_{86}Al_{86}Si_{106}O_{384} \cdot 264\ H_2O$, hereafter referred to as "Na-X zeolite") were used. Their cation exchange capacity (as determined by the "batch exchange method" [37, 38]) was very close to the calculated cation exchange capacity of 5.48 and 4.73 meqg-1 for A and X zeolite, respectively. The grain size distribution curve of the used Na-A zeolite reported in ref. [39], showed: (1) average particles diameter of about 10-12 μm; (2) about 90 wt.% particles with grain size below 21 μm; (3) about 5 wt.% particles with grain size below 1 μm; (4) about 90 wt.% particles with grain size between 5 and 24 μm.
The exchange solution was prepared by dissolving Carlo Erba reagent grade 99.5 wt.% $NiCl_2 \cdot 6\ H_2O$, nickel(II) chloride hexahydrate, in doubly distilled water. The parent A and X zeolites were contacted with a $[Ni^{2+}] = 0.01$ M solution with a solid/liquid weight ratio of 1/100 and contact time (t) = 2 h at about 70°C, in static conditions under continuous stirring. Such a temperature was chosen to improve the exchange efficiency, in agreement with previous studies [25]. The solid was separated from the liquid by filtration, washed with doubly distilled water, dried for about one day at 80°C, and stored for at least 3 days in an environment with about 50 % relative humidity to allow water saturation of the zeolite [40].

Atomic absorption spectrophotometric (AAS) measurements were done using a PerkinElmer Analyst 100 apparatus on materials dissolved in a proper mixture of HF and $HClO_4$ aqueous solution in order to determine the Ni^{2+} and residual Na^+ contents of Ni-exchanged A and X zeolites [41].

Textural properties were determined on the basis of the nitrogen (-196 °C) and carbon dioxide (0 °C) adsorption (Micrometrics ASAP 2020). Before the measurement the sample was outgassed under high vacuum to remove previously adsorbed pollutants. From the isotherm obtained by nitrogen adsorption, the specific surface area S_{BET}, (according to the Brunauer–Emmet–Teller method), micropore volume V_{MP}, (calculated by applying the t-plot method), total pore volume V_P, and pore size distribution (by DFT method-cylindrical pores) have been calculated, while for carbon dioxide isotherm, the specific surface area S_{DR}, and total pore volume have been calculated applying

Dubinin-Radushkevich method.

The amount of water introduced in both samples during ionic exchange was assessed using TGA (LINSEIS STA PT 1600). The temperature was varied from 25 to 900 °C at the rate of 10 °C/min (inert atmosphere with Ar flow 60 ml/min).

X-ray powder diffraction experiment was performed at ID22 beamline of the European Synchrotron Radiation Facility (ESRF) in Grenoble, France using the new Extremely Brilliant Source (EBS). Wavelength was set at 0.354196 Å and 0.354254 Å for Ni^{2+}_A and Ni^{2+}_X samples respectively. Data was collected by an Eiger2 X CdTe 2M-W detector preceded by 13 Si(111) analyser crystals. Structural refinements were performed by using the Topas software in launch mode with Jedit [42]. The starting models for NiA and NiX were taken from [43, 44]. The background was refined using a Chebyshev polynomial, while the profile was modelled using a Thomson pseudo-Voigt function [45]. Soft constraint was applied to Si-O distances (1.65 Å), the position of the extraframework sites was determined through the inspection of the Fourier difference map while their chemical nature was deduced by distances and mutual exclusion rules [46].

Transmission electron microscopy (TEM) and high resolution (HR) TEM analyses were carried out by using a side entry JEOL 3010-UHR microscope operating at 300 kV, equipped with a LaB_6 filament, a (2k×2k)-pixel Gatan US1000 CCD camera and an OXFORD INCA EDS instrument for atomic recognition via energy dispersive spectroscopy (EDS). The samples, in the form of powders, were briefly contacted with a Cu grid with a lacey carbon film, which resulted in the mere electrostatic adhesion of some particles to the sample holder.

Particle size distribution and mean particle diameter (d_m) of NiO were obtained by considering a statistically representative number of particles on different TEM images. The d_m was calculated using the following equation $d_m = \Sigma d_i\ n_i / \Sigma n_i$ where n_i is the number of particles of diameter d_i. Both Ni-exchanged A and X zeolites were stable to prolonged exposition under the electron beam of the instrument (no particle coalescence, nor modification of the zeolitic framework during the measurements).

Magnetic hysteresis loops were measured on Ni-exchanged zeolites using

a Quantum Design MPMS SQUID magnetometer (maximum field: 70 kOe) operating in the temperature range 2 – 300 K. The diamagnetic contribution of both parent zeolites was measured and subtracted from the raw data. FC/ZFC magnetization curves were measured between 2 K and 300 K using the same magnetometer under an applied field of 50 Oe at a constant dT/dt rate of about 6 K/min.

3. RESULTS AND DISCUSSION

According to AAS chemical analysis, sample Ni^{2+}_A contains 1.64 meqg^{-1} Ni^{2+} and 3.75 meqg^{-1} Na^{+}, and sample Ni^{2+}_X contains 2.11 meqg^{-1} Ni^{2+} and 2.54 meqg^{-1} Na^{+}. The corresponding cation equivalent fractions x_{Ni} = 0.31, x_{Na} = 0.69 (sample Ni^{2+}_A), and x_{Ni} = 0.45, x_{Na} = 0.55 (sample Ni^{2+}_X) were calculated. The weight percentage of Ni (wt.% Ni) in the hydrated Ni-exchanged zeolites resulted to be 4.80 (sample Ni^{2+}_A) and 6.20 (sample Ni^{2+}_A).

Finally, the chemical formulas of the Ni-exchanged zeolites were calculated and resulted to be:

Ni^{2+}_A zeolite: $Ni_{1.86}\ Na_{8.28}\ Si_{12}\ Al_{12}\ O_{48} \cdot 24\ H_2O$

Ni^{2+}_X zeolite: $Ni_{19.3}\ Na_{47.3}\ Si_{106}\ Al_{86}\ O_{384} \cdot 214\ H_2O$

In these chemical formulae the exact number of water molecules was determined considering the water content determined through thermogravimetric analysis.

The above reported weight percentages of Ni correspond to N_{ion} = 4.92 $\times 10^{20}$ ions g^{-1} and N_{ion} = 6.36 $\times 10^{20}$ ions g^{-1}, respectively. Using the tabulated mass density values of the zeolites (1.99 g cm^{-3} for zeolite A and 1.91 g cm^{-3} for zeolite X [47]), the corresponding volume concentrations turn out to be: $N_{ion}^{(V)}$ = 9.79 $\times 10^{20}$ ions cm^{-3} and $N_{ion}^{(V)}$ = 1.21 $\times 10^{21}$ ions cm^{-3}.

The textural properties of the exchanged zeolite samples have been evaluated by N_2 and CO_2 adsorption. The N_2 physisorption isotherm of Ni-exchanged zeolite X sample Ni^{2+}_X has a shape resembling the type I according to the IUPAC classifications, typical of microporous structures, Figure 1 (a). However, the presence of a limited desorption hysteresis suggests the presence of small mesopores. The corresponding surface area, evaluated by the BET is reported in Table 1 together with total and micropore volumes.

In the case of Ni-exchanged zeolite A, the resulting BET surface area has been estimated by N_2 adsorption to be less than 10 m^{2}g^{-1} with an isotherm

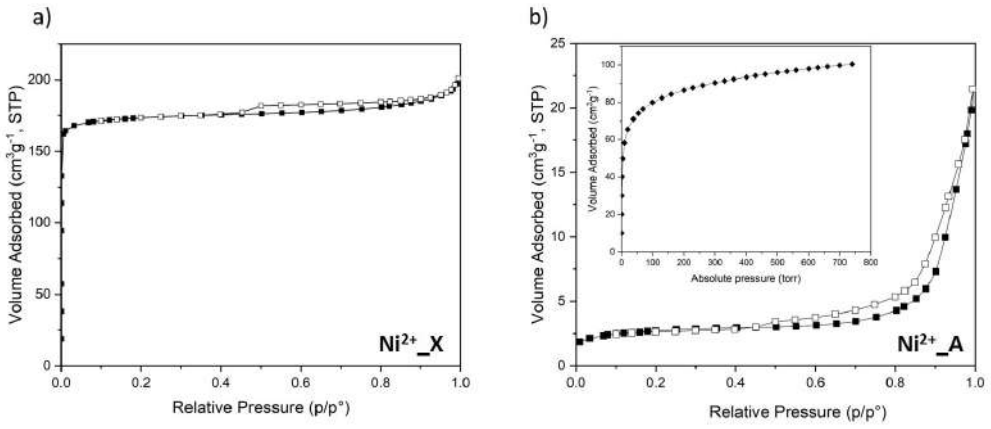

Figure 1: (a) N_2 adsorption isotherms for (a) Ni^{2+}_X and Ni^{2+}_A (b). The inset in panel (b) shows the CO_2 adsorption isotherm.

shape resembling type II, Figure 1 (b). Such an obviously inaccurate estimate of the surface area is explained considering that in this case, the low temperature N_2 adsorption method is inappropriate due to limitation of diffusion related to the kinetic of the probe molecule, the micropores being very narrow [48].
To overcame this issue, CO_2 adsorption at 0 °C was performed on Ni^{2+}_A sample (inset in Figure 1 (b)) [49]. The resulting surface area is now almost coincident with the one measured on sample Ni^{2+}_X (see Table 1).The comparison between both nitrogen and carbon dioxide adsorption analysis allows a deeper investigation of sample properties. In contrast with N_2 adsorption branch, the CO_2 isotherm shape resembles type I, suggesting the presence of very narrow micro porosity and a high surface area calculated by Dubinin-Radushkevich method, Table 1. It is worth noting that for both samples the presence of Ni^{2+} does not appear to affect the textural properties of the pristine zeolites, being the areas comparable with those of the starting zeolites A and X (surface area data not reported for pristine zeolite).

TGA measurements are reported in Figure 2. The Ni^{2+}_A sample lost ca. 20 wt. %: a 17wt. % loss occurred in the 25-200 °C range due to the release of physisorbed water, while an additional loss of 3 wt. % was observed in the range 200-400 °C. The same behaviour can be observed for Ni^{2+}_X

	N_2 (-196 °C)			CO_2 (0 °C)	
	S_{BET} (m^2g^{-1})	V_{MP} (cm^3g^{-1})	V_P (cm^3g^{-1})	S_{DR} (m^2g^{-1})	V_p (cm^3g^{-1})
Sample	BET[a]	t-plot[b]	Total	DR[c]	DR[c]
Ni^{2+}_X	439	0.25	0.31	-	-
Ni^{2+}_A	8	-	0.03	438	0.18

[a] Brunauer-Emmet-Teller. [b] t-plot method. [c] Dubinin-Radushkevich.

Table 1: Textural properties of the Ni^{2+}_X and Ni^{2+}_A samples.

sample, even if with a slight increase in total weight loss (ca. 22 wt. % up to 400 °C).These water losses were found to be consistent with literature data [50]. It should be remarked that high temperature treatments are expected to strongly modify the structure of ion-exchanged zeolites resulting in metal-ceramic nanocomposites that contain Ni^0 nanoparticles, as indeed observed in similar systems after high temperature annealing under reducing atmosphere [27].

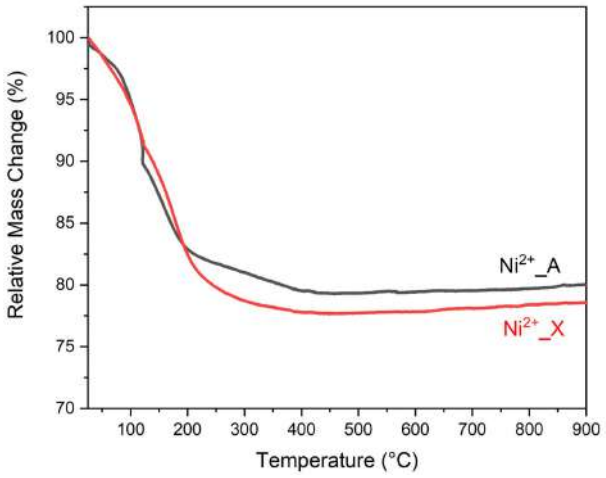

Figure 2: TG curves of Ni^{2+}_A (black line) and Ni^{2+}_X (red line), as obtained under inert atmosphere in the 25-900 °C temperature range.

Structures obtained for samples Ni^{2+}_A and Ni^{2+}_X are reported in panels a), b) of Figure 3 and in Tables S1 and S2 (see Supplementary material),

while observed and calculated diffraction patterns are shown in panels c), d) of Figure 3. Analysis of Ni^{2+}_A zeolite allows one to determine the structural modification resulting from the exchange between sodium and nickel. In particular, 0.95(2) Ni cations are positioned in site (0,0,0), not occupied in the original zeolite, while other cations (0.91) share with sodium the cationic sites in 6MR window and the 8MR window. However, on the basis of the calculated total electronic density, we deduce that a portion of cations (26 electrons) migrates from the original positions into the LTA cage, sharing the position with some H_2O molecules. In sample Ni^{2+}_X, the cation positions of the not-exchanged zeolite are now shared by Ni and Na; in addition, on the basis of the calculated total electronic density, a site or different sites in the main channel, originally occupied by H_2O molecules only, are now occupied by both cations.

HRTEM analyses were carried carried out on both Ni^{2+}_A (Figure 4) and Ni^{2+}_X (Figure 5) samples to investigate possible morphological changes on the commercial zeolites induced by the introduction of Ni. In particular, the observation of the Ni^{2+}_A sample reveals the presence of diffraction fringes on large regions of the zeolitic particles (Figure 4a), corresponding to the 100 plane of the cubic phase (JCPDS file number 00-038-0241) of sodium aluminum silicate hydrate, which means that the insertion of Ni did not alter the crystallinity of zeolite A. Moreover, highly dispersed, ultra-small Ni-containing nanoparticles, as revealed by the EDS analysis, which appear as roundish darker circles with respect to the crystalline zeolitic framework (Figure 4d) with mean diameter $d_m = 1.8 \pm 0.3$ nm were observed (Figure 4, a-c). Considering (i) the preparation procedure that encompasses aging in 50% moisture atmosphere for three days, (ii) the poor contrast in the HRTEM images, (iii) the exposition to air, these nanoparticles are likely made of Ni oxides/hydroxides. The EDS mapping showed the homogeneous relative spatial distribution of Ni cations within the zeolite framework, as measured in several regions of the material (examples are reported in Figure 4f and S1 of the Supplementary material) along with the presence of residual Na^+ cations, which possibly did not contribute to the Ni exchange. It should be remarked that the presence of residual Na^+ cations is not related to an insufficient concentration of Ni in the initial solution. In fact, also in the case of materials containing a much higher fraction of exchanged Ni ions (such as about 15 % [51]) the samples were observed by AAS chemical analysis to still contain an appreciable fraction of Na^+ ions (not less than 1.00 $meqg^1$ in both A and X zeolites [51]). This feature is reasonably related to the

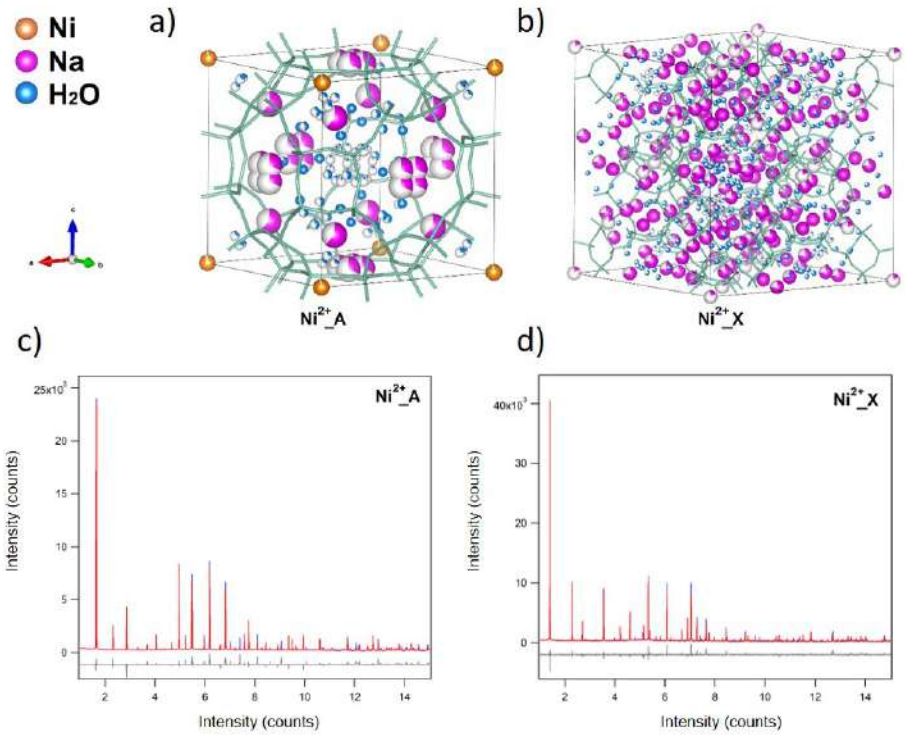

Figure 3: Panels a) and b): structure of Ni^{2+}_A and Ni^{2+}_X samples, respectively. In both zeolites, nickel can be present also in sodium sites; moreover, some cations can be placed in one of the positions originally occupied by the sole H_2O molecules. Panels c) and d): observed (blue line) and calculated (red line) diffraction patterns and final difference curve (grey line) from Rietveld refinement for Ni^{2+}_A and Ni^{2+}_X samples, respectively.

position of Na^+ cations within the zeolite framework, which determines the actual degree of accessibility by the Ni species.

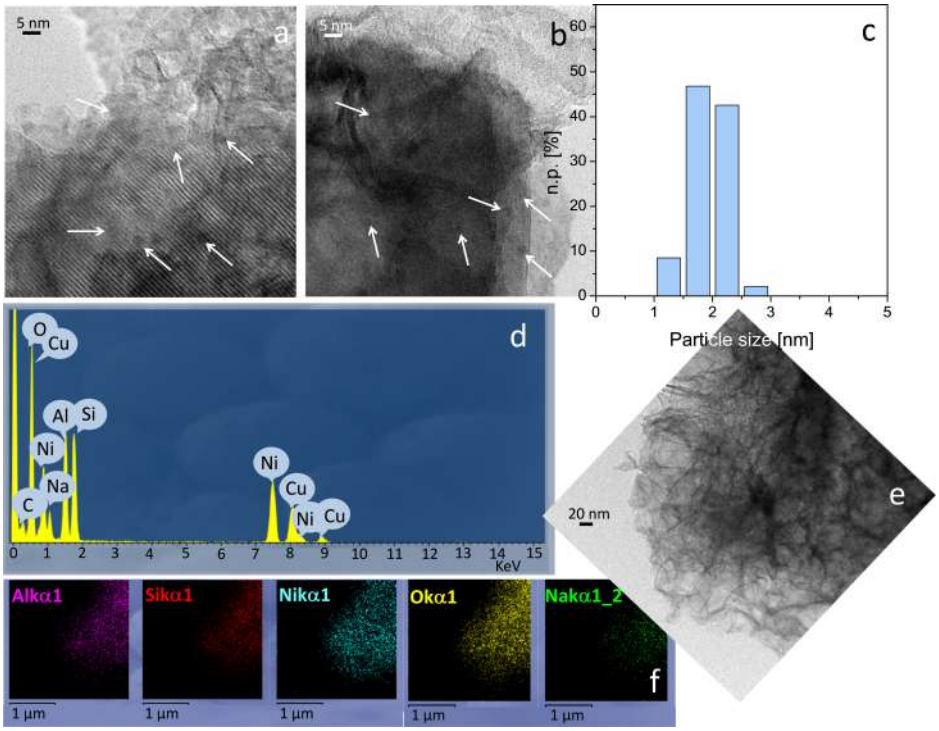

Figure 4: Representative HRTEM (a) and TEM (b,e) images of the Ni^{2+}_A sample and Ni-containing particle size distribution (c). EDS spectrum collected on the region shown in panel b (d). EDS maps of the region shown in panel e (f). The Ni-containing nanoparticles are highlighted by with arrows. Instrumental magnification: 250000× (a and b) and 50000× (e).

The exchanged the Ni^{2+}_X sample displays similar features, i.e. homogeneous Ni distribution within the X zeolite and presence of ultra-small Ni-containing nanoparticles with mean diameter $d_m = 1.3 \pm 0.2$ nm (Figure 5c and Figure S2 of Supplementary material). Also in this case, crystalline regions were observed, as shown in Figure 5 (a,b) in which the diffraction fringes were ascribed to the (111) plane of cubic sodium aluminum silicate hydrate ($Na_{88}Al_{88}Si_{104}O_{384}$ $220H_2O$, JCPDS file number 00-002-0062).

No particular evidence for effects of amorphization of the zeolite structure upon ionic exchange was found in our samples, in contrast with the results

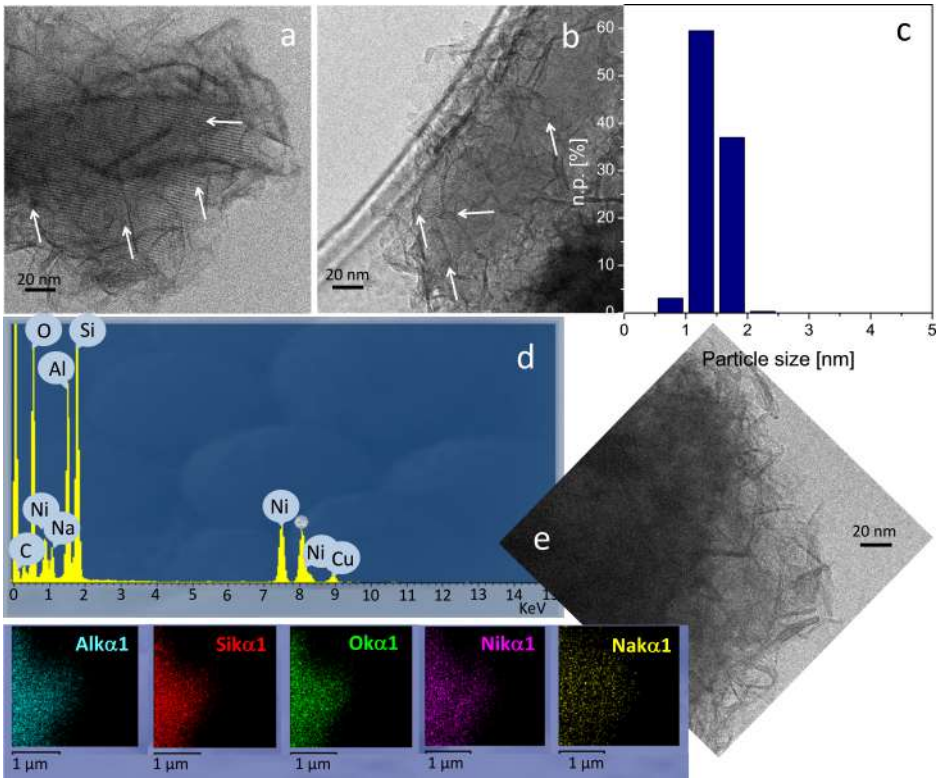

Figure 5: Representative HRTEM (a and b) and TEM (e) images of the Ni^{2+}_X sample and Ni-containing particle size distribution (c). EDS spectrum collected on the region shown in panel b (d). EDS maps of the region shown in panel e (f). The Ni-containing nanoparticles are highlighted by with arrows. Instrumental magnification: 100000×.

discussed in Ref. [25]. Such a different behaviour can be explained taking into account that the amorphization was observed after repeated exchange processes in the presence of a high molar concentration of magnetic cations in the exchange solution (in the present case, only one exchange was performed with a molar concentration one order of magnitude lower than in Ref. [25]). Nevertheless, the concentration of Ni cations incorporated in our samples is large enough to give rise to easily measurable magnetic properties.

Magnetic hysteresis loops measured between -70 and +70 kOe at fixed temperatures in the interval 2-300 K are shown in Figure 6 (a,b). Details of the low-field region below 30 K are shown in (c,d) panels. A nonzero coercive field H_c is observed below about 10 K only, its value strongly increases with decreasing temperature. At high temperatures (50 K $\lesssim$ T $\leq$ 300 K), the $M(H)$ curves are straight lines, whilst a definite downward curvature begins to be observed below 50 K.

The low-field magnetic susceptibility χ_0 was obtained from the $M(H)$ curves in the same interval of temperatures. The quantity χ_0^{-1} is reported as a function of T in Figure 7. In both Ni-exchanged zeolites, χ_0^{-1} follows the Curie-Weiss law above about 20 K; extrapolation of the two fitting straight lines leads to similar Curie temperatures θ = 11.5 K for Ni^{2+}_A and θ = 10.3 K for Ni^{2+}_X, indicating a weak, predominantly ferromagnetic interaction among ions.

Direct exchange can be excluded as the main origin of this ferromagnetic interaction, owing to the rather high interionic distance (which can be estimated from $N_{ion}^{(V)}$ and turns out to be 1.00 and 0.94 nm in Ni^{2+}_A and Ni^{2+}_X, respectively). It is possible that the ferromagnetism in these materials is superexchange-mediated [30].

Fitting the inverse susceptibility to the Curie-Weiss law, the following values of the effective magnetic moment per Ni^{2+} ion result: μ_{eff} = 2.87 μ_B for Ni^{2+}_A and μ_{eff} = 2.83 μ_B for Ni^{2+}_X. These values are compatible with a spin-only contribution to the effective magnetic moment, indicating almost complete (Ni^{2+}_A) or complete (Ni^{2+}_X) quenching of the orbital moment in these materials ([52]); values of the effective magnetic moment ranging from 2.92 and 3.48 μ_B were found in Ni-containing zeolitic structures at different degrees of hydratation [29].

FC/ZFC magnetization curves were measured in both materials in the temperature interval 2-300 K under a field of 50 Oe. The experimental

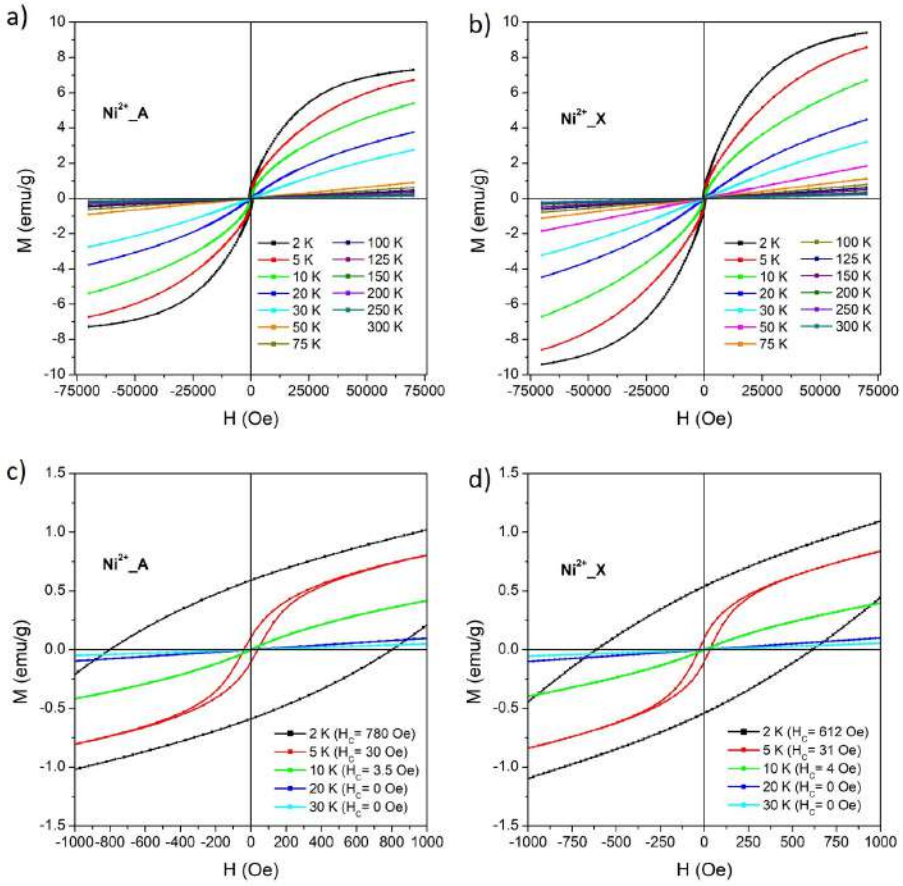

Figure 6: Panels a), b): isothermal hysteresis loops of the two Ni-exchanged zeolites in the 2-300 K temperature range; panels c), d): low-field region at low temperatures; the values of the coercive field H_c are indicated.

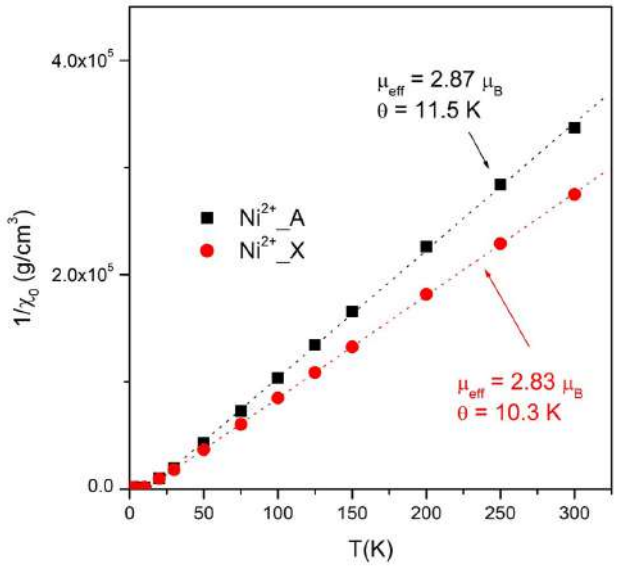

Figure 7: Inverse of the initial susceptibility as a function of temperature in Ni-exchanged zeolites. θ is the paramagnetic Curie temperature.

results in the interval 2-25 K are shown in Figure 8, the curves being perfectly superimposed at higher temperatures. Well below θ, all curves show a behaviour closely similar to the one of a system of magnetic nanoparticles which undergo magnetic blocking. In particular, the ZFC curves display a definite maximum T_M at similar temperatures ($T_M \simeq 6.7$ K for Ni^{2+}_A and $T_M \simeq 6.2$ K for Ni^{2+}_X), clearly indicating magnetic blocking, whilst above the temperature where the ZFC and FC curves merge ($\simeq 8$ K in both materials) thermal equilibrium is attained [53]. This result indicates that the ferromagnetically ordered phase below θ is not a homogeneous one (no long-range ferromagnetic ordering of ionic moments is observed); rather, a nanoparticle-like regime of ferromagnetically ordered arrangements of ions at the nanoscale (hereafter defined as *clusters*) sets up. These clusters, whose average size is estimated below, are characterized by an intrinsic net magnetization and a magnetic anisotropy and therefore can be likened to magnetic nanoparticles characterized by a superparamagnetic regime where magnetization reversal occurs through thermally activated jumps over a local energy barrier, and by a blocked regime at lower temperatures.

In these Ni-exchanged zeolites, a fraction of Ni cations belong in the ultra-small (1-2 nm) nanoparticles put in evidence by HRTEM and deemed to be made of Ni oxides/hydroxides (see Figures 4 and 5). The magnetic properties of nanosized Ni oxide [54, 55, 56] and Ni hydroxide [57, 58, 59] have been investigated by various groups in some papers; order-disorder magnetic transitions and/or particle blocking effects at low temperatures have been described. However, in these works the size of Ni-containing nanoparticles (3-10 nm or more [56]) was systematically larger than the ones measured in our samples. The only evidence regarding ultra-small Ni-containing aggregates (specifically, 2-nm NiO nanoparticles) was that in this case magnetic blocking effects were not observed down to 2 K, and the magnetic response of Ni cations was basically paramagnetic, i.e., not displaying any evidence of magnetic phase transitions [54, 56]. On this basis, it is assumed here that the ultra-small particles evidenced by HRTEM are not characterized by an inner magnetic order down to the lower limit of the investigated temperature range (2 K), so that the constituent Ni^{2+} ions behave not differently from the other paramagnetic Ni cations in the zeolitic structure. In other words, the ultra-small Ni-containing particles, although morphologically distinct from the zeolitic scaffold, do not possess any definite *magnetic* identity; as a consequence, the constituent magnetic cations are submitted to the same collective ordering effects involving the rest of magnetic ions and may take part as well in the magnetic clusters which are formed below the Curie temperature θ.

The sharp peak of the ZFC curve is associated with a narrow distribution of blocking temperatures $p(T_B)$ for ordering clusters, which can be approximately obtained from the simple formula [60]:

$$p(T \equiv T_B) \simeq -\frac{d}{dT}[M_{FC}(T) - M_{ZFC}(T)] \qquad (1)$$

The corresponding distribution of energy barriers $p(E_B)$, obtained by using $E_B \simeq 25 k_B T_B$ where k_B is the Boltzmann's constant, is reported in Figure 9 for both Ni-exchanged zeolites.

Here we assume $T_M \equiv T_B$. The distribution is nearly symmetrical around the mode, which is located at $E_B \simeq 1.86 \times 10^{-14}$ erg in Ni^{2+}_A and $E_B \simeq 1.79 \times 10^{-14}$ in Ni^{2+}_X; the upper limit of $p(E_B)$ is around 2.5×10^{-14} erg.

An estimate of the average size of a cluster of ferromagnetically aligned ions can be obtained from the coercive field in the limit $T \to 0$. Actually, the

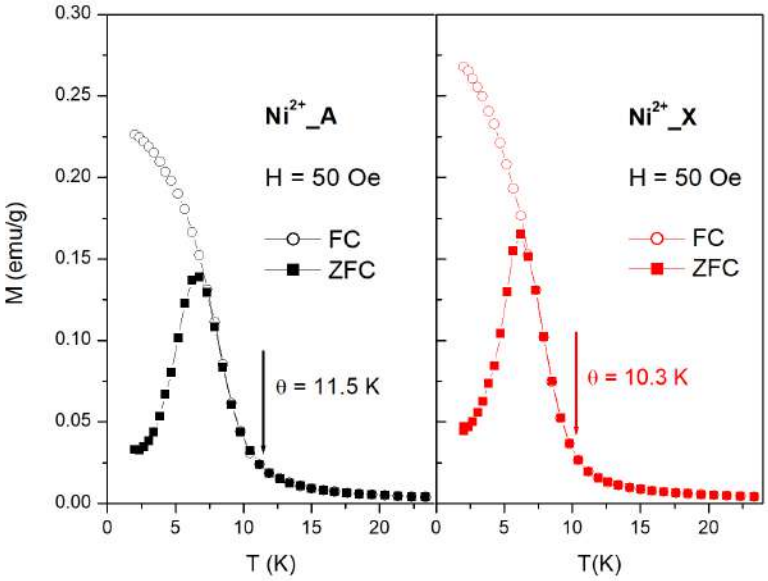

Figure 8: FC/ZFC magnetization curves measured in both materials between 2 K and 25 K under a magnetic field of 50 Oe. The Curie temperature θ is indicated.

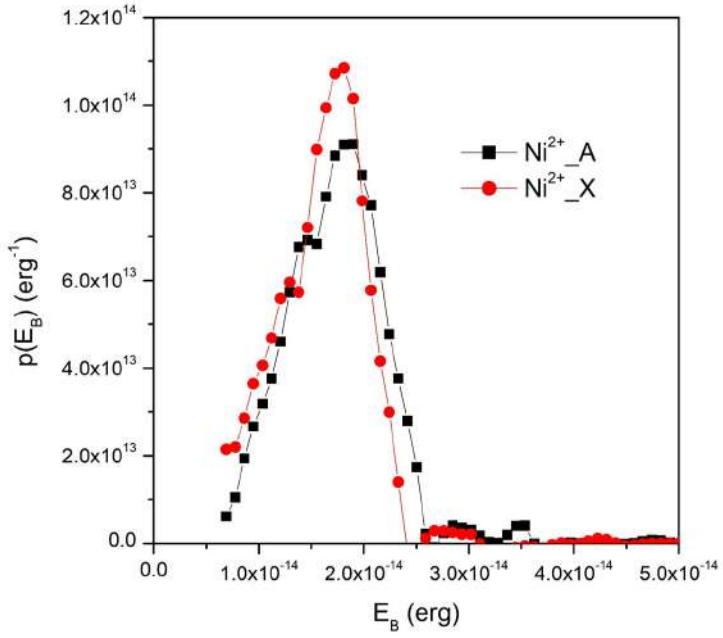

Figure 9: Normalized energy barrier distributions p(E_B) for the two Ni-exchanged zeolites.

coercive field is a very steep function of temperature in the 2-10 K interval, as indicated by the values reported in Figure 6 (c,d). The value of $H_c^{(0)} \equiv H_c(T \to 0)$ is obtained using the theoretical prediction of the rate-equation treatment of magnetic ordering in double-well systems [61]. The extrapolated values are $H_c^{(0)} \simeq 3100$ Oe for Ni^{2+}_A and $\simeq 2500$ Oe for Ni^{2+}_X. In the Stoner-Wohlfarth theory [62], the coercive field of an assembly of blocked nanoparticles may be written as:

$$H_c^{(0)} = 0.96 \frac{< E_B >}{< \mu_{tot} >} \tag{2}$$

where $< \mu_{tot} >$ is the average total magnetic moment of particles and $< E_B >$ is the average energy barrier. This expression can be exploited in order to get the average number of ions per cluster, $< N_{cl} >$.
Assuming full alignment of magnetic moments in a cluster, the total magnetic moment is simply:

$$< \mu_{tot} >=< N_{cl} > \mu_{ion} \tag{3}$$

with $\mu_{ion} = 2.0\ \mu_B$ (the spin-only value of the magnetic moment on Ni^{2+} ions is taken, consistent with the analysis of $\chi_0^{-1}(T)$). As a consequence,

$$< N_{cl} >= 0.96 \frac{< E_B >}{\mu_{ion} H_c^{(0)}} \tag{4}$$

Inserting the parameter values for the two materials, and taking for $< E_B >$ the modal value of the $p(E_B)$ distribution, one gets $< N_{cl} > \simeq$ 310 ions for ionic clusters in Ni^{2+}_A and $\simeq$ 370 for ionic clusters in Ni^{2+}_X. In fact, Eq. 3 applies when the ferromagnetic interaction energy is predominant, leading to perfect alignment of spins in a cluster. However, the magnetic moments of ions in a cluster may not be perfectly aligned, owing to the presence of a non-negligible single-ion magnetic anisotropy with random easy directions, which is competing with a rather weak ferromagnetic interaction. Therefore,$< \mu_{tot} >$ can be smaller than predicted by Eq. 3, and the estimated value of $< N_{cl} >$ greater.
In order to set a minimum value for $< \mu_{tot} >$, it is possible to apply the same line of reasoning used to determine the value of the remanence-to-saturation ratio (M_r/M_s) in bulk ferromagnetic materials [63], the magnetic remanence being defined as the residual magnetization of a ferromagnetic sample when the external field is brought to zero. In that case, magnetic remanence results from the alignment of the local magnetization vector along the easy directions in randomly oriented single grains in the bulk material, whilst in the present case the easy directions correspond to the energy minima for the magnetic moment of single Ni ions in the local crystal field, assumed to be randomly directed within a cluster. In cubic ferromagnetic materials with negative anisotropy, a simple calculation gives $M_r \simeq 0.89\ M_s$ [63]; therefore, the total moment $< \mu_{tot} >$ of a cluster of Ni ions is expected to be reduced by a factor of 0.89 with respect to the value given by Eq. 3 when single-ion anisotropy dominates over the ferromagnetic interaction:

$$< \mu_{tot} > \simeq 0.89 < N_{cl} > \ \mu_{ion}. \tag{5}$$

In this case, the following values of N_{cl} are obtained: 350 ions/cluster for Ni^{2+}_A and 415 ions/cluster for Ni^{2+}_X.
As a consequence, the number of ions per cluster is expected to lie between 310 and 350 and between 370 and 415 for the two Ni-exchanged zeolites, depending on the adopted expression of $< \mu_{tot} >$.
Using the volume concentrations $N_{ion}^{(V)}$, the average size of clusters (approx-

imated to spheres) turns out to be $< D_{cl} > \simeq$ 8.4 - 8.8 nm depending on the values of $< \mu_{tot} >$; remarkably, the cluster size turns out to be basically the same in both materials. It should be noted that the mean size of magnetic clusters turns out to be significantly larger than the one of the Ni-oxide/hydroxide nanoparticles evidenced by HRTEM, confirming that the latter do not play any particular role in the measured blocking effects.

Clusters of correlated ions appear to be characterized by an intrinsic net magnetization (equal to the total moment divided by the cluster volume) and by an effective anisotropy $< K >$ responsible for magnetic blocking. Assuming uniaxial anisotropy, $< K >$ is given by

$$< K >= \frac{< E_B >}{< V_{cl} >}. \tag{6}$$

Therefore, taking the minimum values of $< N_{cl} >$ corresponding to perfect alignment of spins in a cluster, $< K > \simeq 5.85 \times 10^4$ erg/cm^3 for the magnetic clusters in both zeolites. The effective anisotropy is low because it results from the average over local anisotropies with random easy axes within the cluster. Using the random-anisotropy model [64], the anisotropy associated to a single Ni ion in the cluster is estimated to be:

$$K_{ion} = \sqrt{N_{cl}} < K > \tag{7}$$

corresponding to almost equal values in the two zeolites: $K_{ion} \simeq 1.0 \times 10^6$ erg/cm^3 in Ni^{2+}_A and $\simeq 1.1 \times 10^6$ erg/cm^3 in Ni^{2+}_X. Closely similar values for K_{ion} are obtained in the hypothesis of imperfect alignment of spins in a cluster.
It is interesting to note that the first cubic anisotropy constant for Ni^{2+} ions in cubic-tetrahedric sites was measured to be $K_1 \approx 22.5$ cm^{-1}/ion = 0.7 $\times 10^{-15}$ erg/ion for $T \to 0$ [65]. In the studied materials, the values of K_{ion} expressed in erg/ion become $K_{ion} = 1.0 \times 10^{-15}$ erg/ion in Ni^{2+}_A and K_{ion} = 0.9 $\times 10^{-15}$ erg/ion in Ni^{2+}_X. The agreement between these estimates and the experimental value is remarkable and gives support to the present analysis. A summary of the main magnetic parameters of the studied zeolites is given in Table 2. The results turn out to be almost identical in the two zeolites, indicating that the fundamental magnetic properties of the incorporated Ni^{2+} ions are virtually not affected by the structure of the host zeolite.

	Ni^{2+} conc.[a] (wt. %)	μ_{eff}[b] (μ_B)	θ[b] (K)	T_M[c] (K)	$< N_{cl} >$	$< D_{cl} >$ (nm)	$< K >$ (erg/cm^3)	K_{ion} (erg/cm^3)
Ni^{2+}_A	4.8	2.87	11.5	6.7	310-350	8.5-8.8	5.85 $\times 10^4$	1.0×10^6
Ni^{2+}_X	6.2	2.83	10.3	6.2	370-415	8.4-8.7	5.85 $\times 10^4$	1.1×10^6

[a] from AAS. [b] from magnetic susceptibility. [c] from ZFC/FC curves.

Table 2: Magnetic properties of the Ni^{2+}_X and Ni^{2+}_A samples.

On the basis of the information gathered from structural and magnetic measurements, the following description of magnetic phenomena in Ni-exchanged zeolites can be drawn: (i) at high temperatures, the Ni-exchanged zeolites are paramagnetic; however, a weak ferromagnetic interaction among ions exists; (ii) below the Curie temperature θ, no long-range ferromagnetic order sets up; (iii) instead, a nanoparticle-like behaviour is observed, indicating that small clusters of ferromagnetically correlated ions are created; (iv) these clusters have size below 10 nm and typically contain a few hundreds ions; they have a definite identity and are characterized by a net magnetization and an effective anisotropy; (v) as a consequence, the magnetic response of the materials at very low temperatures is determined by the ability of the magnetization of each cluster to reverse its direction by crossing a local energy barrier through thermally activated jumps, resulting in a superparamagnetic-like regime above the blocking temperature and a magnetically blocked state below.

Magnetic clustering at low temperature of Ni^{2+} ions can be explained by making explicit reference to the microscopic mechanisms of ionic exchange of the parent zeolite with the solution containing Ni^{2+} ions, which have been discussed in papers referring to both hydrated and calcined zeolites [66, 67, 68, 69, 70]. In hydrated materials, i.e., prior to any calcination treatment, a fraction of the nickel is considered to be present as fully hydrated cations $[Ni(H_2O)_6]^{2+}$ which are preferentially located in the supercages of the zeolitic LTA or FAU framework, each supercage being big enough to host the hexahydrate Ni^{2+} cluster (the typical diameter of these nanopores is larger than 1 nm) [70]. A simple calculation shows however that in the studied zeolites the available supercages are definitely not in number sufficient to accommodate all of the incorporated nickel: in Ni^{2+}_ A there are about 6.4×10^{20} magnetic ions per gram of zeolite, whilst the number of supercages

is of the order of 3.2×10^{19} per gram of zeolite; in Ni^{2+}_X the corresponding values are 4.9×10^{20} magnetic ions g^{-1} and 3.8×10^{19} magnetic ions g^{-1}, respectively. Therefore, a predominant fraction of the Ni^{2+} ions enters the zeolite scaffold by ionic exchange, each magnetic ion substituting for two Na^{+} ions, as confirmed by X-ray analysis.
In a system with all hexahydrate Ni^{2+} clusters ideally accommodated in supercages in a sort of ordered arrangement, the minimum distance between ions would exceed 2 nm [36] so that magnetic interactions would be basically negligible. As a result, an almost perfect Curie law with a vanishingly small Curie temperature would emerge for $\chi(T)$.
On the contrary, a magnetic interaction among Ni^{2+} ions, albeit rather weak, does exist in both zeolites, as indicated by the paramagnetic Curie-Weiss law with a Curie temperature of 10-11 K. In our view, such an interaction is supported by the exchanged magnetic cations located in the structure between adjacent pores, possibly in favourable sites such as - for instance - II/ II' sites and III*a,b,c* sites of the FAU cell of Zeolite Y [67, 32]. In this case, the minimum distance between adjacent ions can become as low as 0.2 nm, so that the magnetic interaction would be easily transmitted over rather long distances; a possible two-ion mechanism can be superexchange via oxygen, although there is still no well-assessed view about the origin of spin coupling in these insulating solids [30, 32]. In addition, the Ni cations belonging in the ultra-small Ni-oxide/hydroxide particles evidenced by HRTEM also play an important role in sustaining the interaction which results in the formation of magnetic clusters.

The size of magnetic clusters put in evidence at low temperatures by our measurements (8-9 nm) implies that each cluster can contain on the average about 30 ions in hexahydrate state present in the supercages, coupled each other via a substantially larger number of Ni^{2+} ions located in the interposed zeolite scaffold. The concentration of exchanged Ni^{2+} ions in the zeolite scaffold being basically random, magnetic clustering of Ni^{2+} ions will emerge in regions of high local concentration of exchanged magnetic cations, whereas in regions of lower concentration the ions accommodated in neighbouring supercages will remain basically uncoupled because of the lack of a sufficient number of exchanged ions in the zeolite scaffold, which are in turn expected to be almost non-interacting because of the larger mean interdistance.
Therefore, magnetic clusters formed at low temperature are expected to be surrounded by regions where the magnetic cations are basically non-

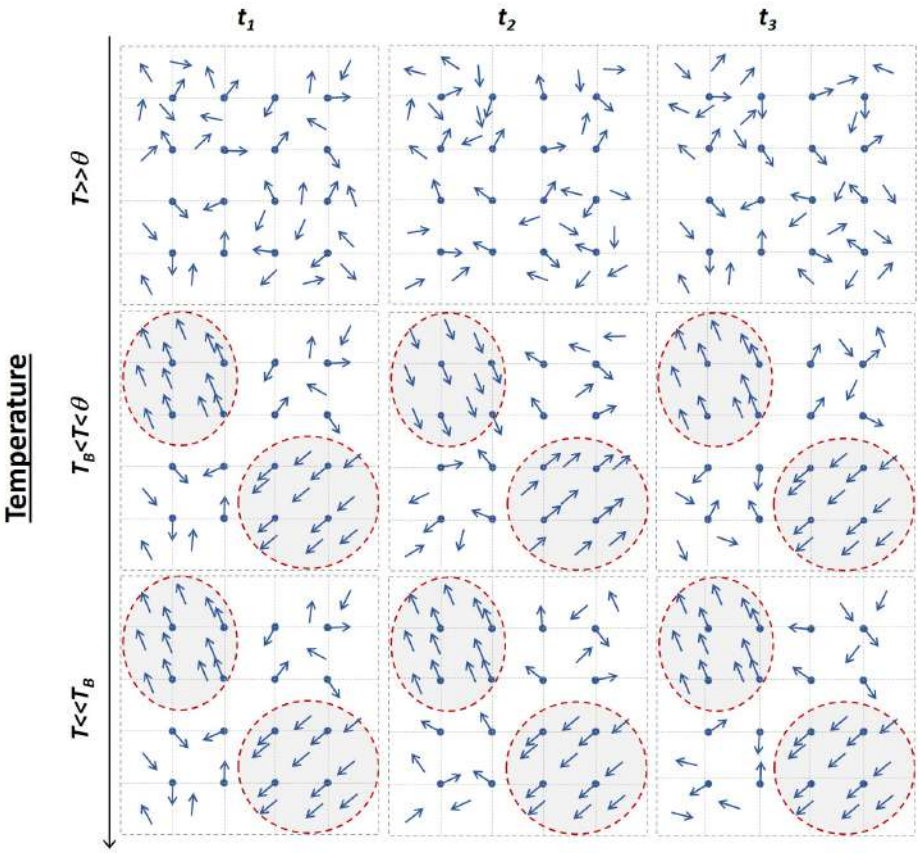

Figure 10: Sketch of the spin arrangement in Ni-exchanged zeolites in different temperature ranges at three arbitrary times t_i (separated by time intervals much larger than the spin-lattice relaxation time). Upper row: paramagnetic state above θ; middle row: superparamagnetic-like regime of ion clusters formed below θ, put in evidence by the different backgound colour, and paramagnetic behaviour of the residual fraction of free ions not belonging in any cluster; bottom row: blocked state of ionic clusters.

interacting, giving support to the present picture of a magnetic interaction favouring the formation of ferromagnetic clusters in the absence of long-range ferromagnetic order. As a consequence, considering the magnetic clusters as statistically independent and basically not interacting with each other is a reasonable starting point.
A simple graphical representation (not to scale) of such a picture is drawn in Figure 10.

4. CONCLUSIONS

Ni-exchanged A and X zeolites, respectively containing 4.8 wt.% and 6.2 wt.% of Ni^{2+} ions exhibit a complex magnetic behaviour which has been investigated by measuring their static magnetic properties. In these materials, hexahydrate Ni^{2+} ions enter the supercages while other Ni^{2+} ions randomly substitute for monovalent Na cations in the zeolitic scaffold; a fraction of magnetic ions belong as well in ultra-small Ni-containing nanoparticles which are created in the exchange process.
The magnetic behaviour of a residual fraction of Ni^{2+} ions was previously observed in Ni-exchanged zeolites submitted to heat treatment with the aim of producing magnetic nanocomposites by effect of the collapse of the zeolitic structure. In that case, however, the magnetic signal arising from a large number of interacting particles of metallic Nickel (Ni^0) generated by thermal treatment was largely predominant, so that disentangling the combined effects of residual ions and of magnetic nanoparticles was a particularly difficult task. Only at very low temperatures were the effects of residual Ni ions actually observed. In those systems, the measurements suggested the onset of blocking effects of magnetic clusters different from Ni^0 nanoparticles, though the available data were sufficient to provide nothing more than a qualitative picture.

On the contrary, measurements done on the present Ni-exchanged zeolites before any thermal treatment are not masked by magnetic effects of Ni^0 nanoparticles, so that the observed effects can be unambiguously ascribed to the response of Ni^{2+} ions.

At high temperatures, all ions give a paramagnetic response (Ni ions belonging in the ultra-small Ni-containing nanoparticles are believed not to

act differently from the other ions incorporated in the zeolites). A weak ferromagnetic interaction, possibly mediated by positive superexchange, exists; such an interaction is responsible for the appearance of a magnetically ordered state below the Curie temperature. However, no evidence has been found for the onset of long-range order; rather, magnetic order must be short-ranged, leading to the formation of ferromagnetically correlated clusters of ions with typical size of 8-9 nm in both zeolites. These clusters encompass several zeolitic cells and contain a few hundreds of magnetic ions, ranging from about 310 to about 415 on the average, in dependence of the type of zeolite and of the degree of alignment of the ionic moments in the cluster.
Magnetic clusters are deemed responsible for the particle-like behaviour observed in the present materials by FC/ZFC measurements. In fact, each cluster is characterized by net magnetization and effective anisotropy so that it may be likened to a magnetic nanoparticle, whose response to a magnetic field is ruled by magnetization reversal through thermally activated jumps over an energy barrier depending on magnetic anisotropy. On the other hand, ionic clusters substantially differ from magnetic nanoparticles because they gradually lose their identity when the Curie temperature is approached from below and finally dissolve into almost independent ions for $T \gtrsim \theta$.
The formation of these ionic clusters indicates that the distribution of magnetic ions in the zeolitic structure is not completely random. In regions of higher density of magnetic ions, the slightly larger magnetic interaction is expected to ease the formation of ferromagnetically correlated clusters. The fluctuation of ionic density must have a wavelength close to the estimated size of ionic clusters.

References

[1] Y. Li, J. Yu, Emerging applications of zeolites in catalysis, separation and host–guest assembly, Nature Reviews Materials (2021). doi:10.1038/s41578-021-00347-3.

[2] X. Zeng, X. Hu, H. Song, G. Xia, Z.-Y. Shen, R. Yu, M. Moskovits, Microwave synthesis of zeolites and their related applications, Microporous and Mesoporous Materials 323 (2021) 111262. doi:https://doi.org/10.1016/j.micromeso.2021.111262.

[3] Y. Li, H. Cao, J. Yu, Toward a New Era of Designed Synthesis of Nanoporous Zeolitic Materials, ACS Nano 12 (5) (2018) 4096–4104. doi:10.1021/acsnano.8b02625.

[4] P. Kumar, D. W. Kim, N. Rangnekar, H. Xu, E. O. Fetisov, S. Ghosh, H. Zhang, Q. Xiao, M. Shete, J. I. Siepmann, T. Dumitrica, B. McCool, M. Tsapatsis, K. A. Mkhoyan, One-dimensional intergrowths in two-dimensional zeolite nanosheets and their effect on ultra-selective transport, Nature Materials 19 (4) (2020) 443–449. doi:10.1038/s41563-019-0581-3.

[5] P. Misaelides, Application of natural zeolites in environmental remediation: A short review, Microporous and Mesoporous Materials 144 (1-3) (2011) 15–18. doi:10.1016/j.micromeso.2011.03.024.

[6] M. Delkash, B. Ebrazi Bakhshayesh, H. Kazemian, Using zeolitic adsorbents to cleanup special wastewater streams: A review, Microporous and Mesoporous Materials 214 (2015) 224–241. doi:10.1016/j.micromeso.2015.04.039.

[7] N. Das, J. K. Das, Zeolites: An Emerging Material for Gas Storage and Separation Applications, Zeolites - New Challenges (2020). doi:10.5772/INTECHOPEN.91035.

[8] X. Chen, X. Lei, H. Zheng, X. Jiang, B. Zhang, H. Zhang, C. Lu, Q. Zhang, Facile one-step synthesis of magnetic zeolitic imidazolate framework for ultra fast removal of congo red from water, Microporous and Mesoporous Materials 311 (2021) 110712. doi:https://doi.org/10.1016/j.micromeso.2020.110712.

[9] N. Kosinov, C. Liu, E. J. Hensen, E. A. Pidko, Engineering of Transition Metal Catalysts Confined in Zeolites, Chemistry of Materials 30 (10) (2018) 3177–3198. doi:10.1021/acs.chemmater.8b01311.

[10] Q. Lv, G. Li, H. Lu, W. Cai, H. Huang, C. Cheng, Preparation of magnetic zeolite γ-fe$_2$o$_3$/ts-1 with core/shell structure and application in photocatalytic degradation, Microporous and Mesoporous Materials 203 (2015) 202–207. doi:https://doi.org/10.1016/j.micromeso.2014.10.040.

[11] B. E. Snyder, P. Vanelderen, M. L. Bols, S. D. Hallaert, L. H. Böttger, L. Ungur, K. Pierloot, R. A. Schoonheydt, B. F. Sels, E. I. Solomon, The

active site of low-temperature methane hydroxylation in iron-containing zeolites, Nature 536 (7616) (2016) 317–321. doi:10.1038/nature19059.

[12] A. Martínez, M. A. Arribas, P. Concepción, S. Moussa, New bifunctional Ni-H-Beta catalysts for the heterogeneous oligomerization of ethylene, Applied Catalysis A: General 467 (2013) 509–518. doi:10.1016/j.apcata.2013.08.021.

[13] K. Lu, F. Jin, G. Wu, Y. Ding, The synergetic effect of acid and nickel sites on bifunctional MWW zeolite catalysts for ethylene oligomerization and aromatization, Sustainable Energy and Fuels 3 (12) (2019) 3569–3581. doi:10.1039/c9se00771g.

[14] A. Ehrmaier, Y. Liu, S. Peitz, A. Jentys, Y. H. C. Chin, M. Sanchez-Sanchez, R. Bermejo-Deval, J. Lercher, Dimerization of Linear Butenes on Zeolite-Supported Ni^{2+}, ACS Catalysis 9 (1) (2019) 315–324. doi:10.1021/acscatal.8b03095.

[15] Y. Chai, G. Wu, X. Liu, Y. Ren, W. Dai, C. Wang, Z. Xie, N. Guan, L. Li, Acetylene-Selective Hydrogenation Catalyzed by Cationic Nickel Confined in Zeolite, Journal of the American Chemical Society 141 (25) (2019) 9920–9927. doi:10.1021/jacs.9b03361.

[16] M. Lopes, T. Coutinho, C. Farinas, Modification of zeolite with metallic ions improves the immobilization of phytase, Biocatalysis and Agricultural Biotechnology 36 (36) (2021) 102137. doi:10.1016/j.bcab.2021.102137.

[17] A. Borgschulte, E. Callini, N. Stadie, Y. Arroyo, M. D. Rossell, R. Erni, H. Geerlings, A. Züttel, D. Ferri, Manipulating the reaction path of the CO_2 hydrogenation reaction in molecular sieves, Catalysis Science & Technology 5 (9) (2015) 4613–4621. doi:10.1039/C5CY00528K.

[18] G. Barrera, P. Tiberto, P. Allia, B. Bonelli, S. Esposito, A. Marocco, M. Pansini, Y. Leterrier, G. Barrera, P. Tiberto, P. Allia, B. Bonelli, S. Esposito, A. Marocco, M. Pansini, Y. Leterrier, Magnetic Properties of Nanocomposites, Applied Sciences 9 (2) (2019) 212. doi:10.3390/app9020212.

[19] M. Pansini, G. Dell'Agli, A. Marocco, P. P. A. Netti, E. Battista, V. Lettera, P. Vergara, P. Allia, B. Bonelli, P. Tiberto, G. Barrera, G. Alberto, G. Martra, R. Arletti, S. Esposito, Preparation and Characterization of Magnetic and Porous Metal-Ceramic Nanocomposites from a Zeolite Precursor and Their Application for DNA Separation, Journal of Biomedical Nanotechnology 13 (3) (2017) 337–348. doi:10.1166/jbn.2017.2345.

[20] S. Esposito, A. Marocco, G. Dell'Agli, B. Bonelli, F. Mannu, P. Allia, P. Tiberto, G. Barrera, M. Pansini, Separation of biological entities from human blood by using magnetic nanocomposites obtained from zeolite precursors, Molecules 25 (8) (2020). doi:10.3390/molecules25081803.

[21] M. Pansini, F. Sannino, A. Marocco, P. Allia, P. Tiberto, G. Barrera, M. Polisi, E. Battista, P. Netti, S. Esposito, Novel process to prepare magnetic metal-ceramic nanocomposites from zeolite precursor and their use as adsorbent of agrochemicals from water, Journal of Environmental Chemical Engineering 6 (1) (2018). doi:10.1016/j.jece.2017.12.030.

[22] A. Marocco, G. Dell'Agli, F. Sannino, S. Esposito, B. Bonelli, P. Allia, P. Tiberto, G. Barrera, M. Pansini, Removal of agrochemicals from waters by adsorption: A critical comparison among humic-like substances, zeolites, porous oxides, and magnetic nanocomposites, Processes 8 (2) (2020). doi:10.3390/pr8020141.

[23] F. S. Freyria, A. Marocco, S. Esposito, B. Bonelli, G. Barrera, P. Tiberto, P. Allia, P. Oudayer, A. Roggero, J.-C. Matéo-Vélez, et al., Simulated moon agglutinates obtained from zeolite precursor by means of a low-cost and scalable synthesis method, ACS Earth and Space Chemistry 3 (9) (2019) 1884–1895.

[24] M. Manzoli, O. Tammaro, A. Marocco, B. Bonelli, G. Barrera, P. Tiberto, P. Allia, J.-C. Matéo-Vélez, A. Roggero, E. Dantras, R. Arletti, M. Pansini, S. Esposito, New Insights in the Production of Simulated Moon Agglutinates: the Use of Natural Zeolite-Bearing Rocks, ACS Earth and Space Chemistry 5 (6) (2021) 1631–1646. doi:10.1021/ACSEARTHSPACECHEM.1C00118.

[25] C. Weidenthaler, W. Schmidt, Thermal stability and thermal transformations of Co^{2+} or Ni^{2+} exchanged zeolites A, X, and Y,

Chemistry of Materials 12 (12) (2000) 3811–3820, cited By 45. doi:10.1021/cm0011312.

[26] J. S. Yoon, M. B. Park, Y. Kim, H. J. Chae, D. W. Hwang, Effect of metal oxide–support interactions on ethylene oligomerization over nickel oxide/silica–alumina catalysts, Catalysts 9 (11) (2019) 20–24. doi:10.3390/catal9110933.

[27] G. Barrera, P. Tiberto, S. Esposito, A. Marocco, B. Bonelli, M. Pansini, M. Manzoli, P. Allia, Magnetic clustering of Ni^{2+} ions in metal-ceramic nanocomposites obtained from Ni-exchanged zeolite precursors, Ceramics International 44 (14) (2018) 17240–17250. doi:10.1016/j.ceramint.2018.06.182.

[28] G. Barrera, P. Allia, B. Bonelli, S. Esposito, F. Freyria, M. Pansini, A. Marocco, G. Confalonieri, R. Arletti, P. Tiberto, Magnetic behavior of Ni nanoparticles and Ni^{2+} ions in weakly loaded zeolitic structures, Journal of Alloys and Compounds 817 (2020). doi:10.1016/j.jallcom.2019.152776.

[29] T. A. Egerton, J. C. Vickerman, Magnetic studies of zeolites. Part 2.—Magnetic properties of NiA, NiX and NiY, Journal of the Chemical Society, Faraday Transactions 1: Physical Chemistry in Condensed Phases 69 (0) (1973) 39–49. doi:10.1039/F19736900039.

[30] L. Tong, F. Wu, S. Yan, T. Ji, B. Lin, Paramagnetic behavior in NiNaY zeolites, Solid State Communi 97 (12) (1996) 1043–1046.

[31] Y. Horikawa, N. Ohnishi, K. Hiraga, Structures and magnetic susceptibility of Ni-ion-introduced zeolite A and X, Materials Science and Engineering A 217-218 (1996) 139–141. doi:10.1016/S0921-5093(96)10318-X.

[32] M. D. Mukadam, S. M. Yusuf, R. Sasikala, Magnetic properties of Ni2+ clusters in NaY zeolite, Journal of Applied Physics 102 (10) (2007) 0–5. doi:10.1063/1.2815624.

[33] S. Ronchetti, E. Turcato, A. Delmastro, S. Esposito, C. Ferone, M. Pansini, B. Onida, D. Mazza, Study of the thermal transformations of co- and fe-exchanged zeolites a and x by "in situ" xrd under reducing atmosphere, Materials Research Bulletin 45 (6) (2010) 744–750. doi:10.1016/j.materresbull.2010.02.006.

[34] A. Marocco, G. Dell'Agli, S. Esposito, M. Pansini, Metal-ceramic composite materials from zeolite precursor, Solid State Sciences 14 (3) (2012) 394–400. doi:10.1016/j.solidstatesciences.2012.01.006.

[35] S. Esposito, G. Dell'Agli, A. Marocco, B. Bonelli, P. Allia, P. Tiberto, G. Barrera, M. Manzoli, R. Arletti, M. Pansini, Magnetic metal-ceramic nanocomposites obtained from cation-exchanged zeolite by heat treatment in reducing atmosphere, Microporous and Mesoporous Materials 268 (2018) 131–143.

[36] D. O. Ch. Baerlocher, Lynne B. McCusker, Atlas of Zeolite Framework Types (2007).

[37] A. Marocco, G. Dell'Agli, L. Spiridigliozzi, S. Esposito, M. Pansini, The multifarious aspects of the thermal conversion of Ba-exchanged zeolite A to monoclinic celsian, Microporous and Mesoporous Materials 256 (2018) 235–250. doi:10.1016/j.micromeso.2017.08.018.

[38] N. J. Clayden, S. Esposito, C. Ferone, M. Pansini, ^{29}Si and ^{27}Al NMR study of the thermal transformation of barium exchanged zeolite-A to celsian, Journal of Materials Chemistry 13 (7) (2003) 1681–1685. doi:10.1039/B212717B.

[39] A. Marocco, B. Liguori, G. Dell'Agli, M. Pansini, Sintering behaviour of celsian based ceramics obtained from the thermal conversion of (Ba, Sr)-exchanged zeolite A, Journal of the European Ceramic Society 31 (11) (2011) 1965–1973. doi:10.1016/j.jeurceramsoc.2011.04.028.

[40] A. Colantuono, S. Dal Vecchio, G. Mascolo, M. Pansini, Thermal shrinkage of various cation forms of zeolite A, Thermochimica Acta 296 (1997) 59–66.

[41] C. Colella, M. Pansini, Lead removal from wastewaters using chabazite tuff, ACS Symposium Series (368) (1988) 500–510. doi:10.1021/bk-1988-0368.ch032.

[42] A. Coelho, Topas and topas-academic: An optimization program integrating computer algebra and crystallographic objects written in c++: An, Journal of Applied Crystallography 51 (1) (2018) 210–218. doi:10.1107/S1600576718000183.

[43] H. Luhrs, J. Derr, R. Fischer, K and ca exchange behavior of zeolite a, Microporous and Mesoporous Materials 151 (15) (2012) 457–465. doi:10.1016/j.micromeso.2011.09.025.

[44] R. Arletti, L. Gigli, F. Di Renzo, S. Quartieri, Evidence for the formation of stable co2 hydrates in zeolite na-y: Structural characterization by synchrotron x-ray powder diffraction, Microporous and Mesoporous Materials 228 (2016) 248–255. doi:10.1016/j.micromeso.2016.03.046.

[45] P. Thompson, D. Cox, J. Hastings, Rietveld refinement of debye–scherrer synchrotron x-ray data from al2o3 20 (2) (1987) 79–83. doi:10.1107/S0021889887087090.

[46] G. Confalonieri, A. Ryzhikov, R. Arletti, H. Nouali, S. Quartieri, T. Daou, J. Patarin, Intrusion-extrusion of electrolyte aqueous solutions in pure silica chabazite by in situ high pressure synchrotron x-ray powder diffraction 122 (49) (2018) 28001–28012. doi:10.1021/acs.jpcc.8b07338.

[47] D. Breck, Zeolite Molecular Sieves: Structure, Chemistry and Uses, Wiley, New York, 1974.

[48] K. J. Hwang, W. S. Choi, S. H. Jung, Y. J. Kwon, S. Hong, C. Choi, J. W. Lee, W. G. Shim, Synthesis of zeolitic material from basalt rock and its adsorption properties for carbon dioxide, RSC Advances 8 (17) (2018) 9524–9529. doi:10.1039/c8ra00788h.

[49] R. M. Mohamed, A. A. Ismail, G. Kini, I. A. Ibrahim, B. Koopman, Synthesis of highly ordered cubic zeolite A and its ion-exchange behavior, Colloids and Surfaces A: Physicochemical and Engineering Aspects 348 (1-3) (2009) 87–92. doi:10.1016/j.colsurfa.2009.06.038.

[50] S. Esposito, A. Marocco, G. Dell'Agli, B. De Gennaro, M. Pansini, Relationships between the water content of zeolites and their cation population, Microporous and Mesoporous Materials 202 (2015) 36–43. doi:10.1016/j.micromeso.2014.09.041.

[51] S. Esposito, G. Dell'Agli, A. Marocco, B. Bonelli, P. Allia, P. Tiberto, G. Barrera, M. Manzoli, R. Arletti, M. Pansini, Magnetic metal-ceramic nanocomposites obtained from cation-exchanged zeolite by heat treatment in reducing atmosphere, Microporous and Mesoporous Materials 268 (2018) 131–143. doi:10.1016/J.MICROMESO.2018.04.024.

[52] J. M. D. Coey, Magnetism and Magnetic Materials, Cambridge University Press, Cambridge, 2009.

[53] P. Allia, G. Barrera, P. Tiberto, Linearized rate-equation approach for double-well systems: Cooling- and temperature-dependent low-field magnetization of magnetic nanoparticles, Physical Review B 98 (2018) 134423. doi:10.1103/PhysRevB.98.134423.

[54] J. Park, E. Kang, S. U. Son, H. M. Park, M. K. Lee, J. Kim, K. W. Kim, H. J. Noh, J. H. Park, C. J. Bae, J. G. Park, T. Hyeon, Monodisperse nanoparticles of Ni and NiO: Synthesis, characterization, self-assembled superlattices, and catalytic applications in the suzuki coupling reaction, Advanced Materials 17 (4) (2005) 429–434. doi:10.1002/adma.200400611.

[55] J. B. Yi, J. Ding, Y. P. Feng, G. W. Peng, G. M. Chow, Y. Kawazoe, B. H. Liu, J. H. Yin, S. Thongmee, Size-dependent magnetism and spin-glass behavior of amorphous NiO bulk, clusters, and nanocrystals: Experiments and first-principles calculations, Physical Review B - Condensed Matter and Materials Physics 76 (22) (2007) 2–6. doi:10.1103/PhysRevB.76.224402.

[56] M. Tadic, D. Nikolic, M. Panjan, G. R. Blake, Magnetic properties of NiO (nickel oxide) nanoparticles: Blocking temperature and Neel temperature, Journal of Alloys and Compounds 647 (2015) 1061–1068. doi:10.1016/j.jallcom.2015.06.027.
URL http://dx.doi.org/10.1016/j.jallcom.2015.06.027

[57] Y. Ichiyanagi, Y. Kimishima, Magnetic and structural studies of ni(oh)$_2$ monolayered nanoclusters, Jpn. J. Appl. Phys. 35 (4A) (1996) 2140–2144. doi:10.1063/1.3374468.

[58] Y. Ichiyanagi, Y. Kimishima, Magnetic properties of 2D ising mesoscopic ferromagnet $Ni(OH)_2$ monolayer nanoclusters, Journal of Magnetism and Magnetic Materials 177-181 (PART 2) (1998) 964–965. doi:10.1016/S0304-8853(97)00970-0.

[59] X. H. Liu, W. Liu, X. K. Lv, F. Yang, X. Wei, Z. Zhang, D. J. Sellmyer, Magnetic properties of nickel hydroxide nanoparicles, Journal of Applied Physics 107 (083919) (2010) 1–3. doi:10.1063/1.3374468.

[60] H. Mamiya, M. Ohnuma, I. Nakatani, T. Furubayashim, Extraction of blocking temperature distribution from zero-field-cooled and field-cooled magnetization curves, IEEE Transactions on Magnetics 41 (10) (2005) 3394–3396. doi:10.1109/TMAG.2005.855205.

[61] P. Allia, G. Barrera, P. Tiberto, Hysteresis effects in magnetic nanoparticles: A simplified rate-equation approach, Journal of Magnetism and Magnetic Materials 496 (2020). doi:10.1016/j.jmmm.2019.165927.

[62] G. Bertotti, Hysteresis in Magnetism: For Physicists, Materials Scientists, and Engineers (1998). arXiv:arXiv:1011.1669v3.

[63] S. Chikazumi, Physics of Ferromagnetism, Oxford University Press, Oxford, 1997.

[64] G. Herzer, Grain size dependence of coercivity and permeability 26 (5) (1990) 1397–1402.

[65] A. J. Pointon, J. M. Robertson, G. A. Wetton, Anisotropy of Ni^{2+} and Ni^{3+} ions in cubic sites, Le Journal de Physique Colloques 32 (1971) C1–850–C1–852. doi:10.1051/jphyscol:19711297.

[66] P. Gallezot, B. Imelik, Location of Nickel Ions in Y Zeolites. 1. Influence of Thermal Treatment, Journal of Physical Chemistry 295 (101) (1972) 652–656.

[67] J. M. Thomas, C. Williams, T. Rayment, Monitoring cation-site occupancy of nickel-exchanged zeolite Y catalysts by high-temperature in situ X-ray powder diffractometry, Journal of the Chemical Society, Faraday Transactions 1: Physical Chemistry in Condensed Phases 84 (9) (1988) 2915–2931. doi:10.1039/F19888402915.

[68] B. Coughlan, M. A. Keane, Reduction of Ni^{2+} cations in Y zeolites. I. Effect of sample pretreatment, Journal of Catalysis 123 (2) (1990) 364–374. doi:10.1016/0021-9517(90)90135-7.

[69] E. Dooryhee, C. R. Catlow, J. W. Couves, P. J. Maddox, J. M. Thomas, G. N. Greaves, A. T. Steel, R. P. Townsend, A study of cation environment and movement during dehydration and reduction of nickel-exchanged zeolite Y by X-ray absorption and diffraction, Journal of Physical Chemistry 95 (11) (1991) 4514–4521. doi:10.1021/j100164a062.

[70] W. Louisfrema, J. L. Paillaud, F. Porcher, E. Perrin, T. Onfroy, P. Massiani, A. Boutin, B. Rotenberg, Cation Migration and Structural Deformations upon Dehydration of Nickel-Exchanged NaY Zeolite: A Combined Neutron Diffraction and Monte Carlo Study, Vol. 120, 2016. doi:10.1021/acs.jpcc.6b05657.